IPPP/12/35
DCPT/12/70
IFJPAN-IV-2012-1

Gluon saturation in dijet production in p-Pb collisions at Large Hadron Collider

Krzysztof Kutak
Instytut Fizyki Jądrowej im. Henryka Niewodniczańskiego
Radzikowskiego 152, 31-342 Kraków, Poland

Sebastian Sapeta
Institute for Particle Physics Phenomenology, Durham University,
South Rd, Durham DH1 3LE, UK

Abstract

We study saturation effects in the production of dijets in p-p and p-Pb collisions using the framework of *high energy factorization*. We focus on central-forward jet configurations, which allow for probing gluon density at low longitudinal momentum fraction. We find significant suppression of the central-forward jet decorrelations in p-Pb compared to p-p, which we attribute to saturation of gluon density in nuclei.

1 Introduction

Physics in the forward region at the Large Hadron Collider (LHC) is a very interesting and exciting field since it involves interplay of the kinematical scales, like for example transverse momenta of jets, with scales generated by the QCD dynamics, like the saturation scale Q_s [1]. The latter scale characterizes formation of dense system of partons and there is a growing evidence that the phenomenon of saturation of gluons indeed occurs [2–5]. To further advance studies of saturation and other possible effects occurring at high partonic density, the LHC is going to collide p-Pb this year. This will allow, in particular, for the study of the onset of saturation as a function of variables related to the transverse momentum p_t of jets. In addition, the understanding of the interplay of scales in the jet production in p-p and p-Pb will permit to constrain the unintegrated parton densities in the large phase space available for partons, i.e. $10^{-6} < x < 0.1$, $5\,\mathrm{GeV} < k_t < 150\,\mathrm{GeV}$, where x is the longitudinal momentum fraction of the hadron carried by a parton, while k_t is the component of its momentum transverse to the collision axis. In particular, the study of exclusive final states, like jets, allows for determination of the unintegrated gluon density in the range of large momenta.

There are formalisms that allow one to study dense systems [6] or systems with hard momentum scale involved [7]. However, the formalism which accounts for both the high energy scale and the hard momentum scale p_t is provided only by the *high energy factorization* [8]. In this framework, one of the elements that enter the factorization formula is the unintegrated gluon

density. Depending on approximation, it satisfies the BFKL, BK, or CCFM evolution equations [9–16]. The BFKL and BK equations are known already at NLO and sum up emissions of gluons with strong ordering in the longitudinal momentum fractions of subsequently emitted gluons. The important issue for phenomenological applications, in particular for exclusive final states at large p_t, is to perform resummations of most relevant higher order corrections to the evolution kernel of the BFKL equation. This is because only then, the solution of the equation for the unintegrated gluon density is physically relevant and well defined [17–19].

Another issue is that since the BFKL or CCFM equation are linear they predict strong rise of gluon density at small values of gluon's k_t which leads to conflict with unitarity bounds. Effects of higher orders, although suppress the growth of gluon density, preserve its power like behavior as a function of k_t at low k_t values. To restore unitarity one supplements the BFKL equation with a nonlinear term which accounts for fusions of gluons. These unitarity corrections, which are taken into account in the BK or JIMWLK equations, give rise to an emergent semi-hard scale, called the saturation scale $Q_s(x)$, at which the gluon density has a maximum and which therefore defines the most probable momentum of gluon [20, 21].

An interesting process in which both saturation and production at high p_t can be studied, is the process of dijet production where the jets are separated by large rapidity [22–25]. More specifically, we shall focus on the case in which one jet is in the central while the other in the forward rapidity region. Such a final state probes parton density of one of the protons at low longitudinal momentum fraction x while the other at large longitudinal momentum fraction. The latter proton can be described by the well known collinear parton distribution functions and therefore such process is perfectly suited to study properties of the unintegrated gluon density at low x and especially its saturation.

In this paper, we discuss production of dijets in the p-p and p-Pb collisions. The former serves as a benchmark, i.e. first we fit the unintegrated gluon density to the F_2 data [26] and then apply it to calculate observables in p-p characterizing the dijet system like angular correlations of produced jets, p_t spectra of forward and central jets and their rapidity distributions. In the next step we compute predictions for rapidity distributions and angular decorrelations of central-forward jets produced in p-Pb collision. For both observables we see significant suppression of the cross section due to saturation effects in the nucleus.

The paper is organized as follows. In section 2 we introduce the *high energy factorization* framework and define the observables we want to use as a tool to study saturation effects. In section 3 we introduce the unified BK/DGLAP equation [27] for the unintegrated gluon density and present results of fits of the unintegrated gluon to the combined HERA data. In section 4 we apply the high energy factorization framework together with our fitted unintegrated gluon to calculate observables for central-forward dijet system. In the section 5 we calculate rapidity distribution and angular decorrelations of central-forward jets produced in p-Pb collision. We conclude our studies in section 6.

2 Dijet production in high energy factorization approach

The main goal of this paper is to provide predictions for azimuthal decorrelations of jets produced in p-p and p-Pb collisions. Consider the process of the production of a dijet system in the collision of two hadrons

$$A + B \to J_1 + J_2 + X\,. \tag{2.1}$$

The leading order contribution comes from the $2 \to 2$ partonic process

$$a(k_1) + b(k_2) \to c(p_1) + d(p_2)\,. \tag{2.2}$$

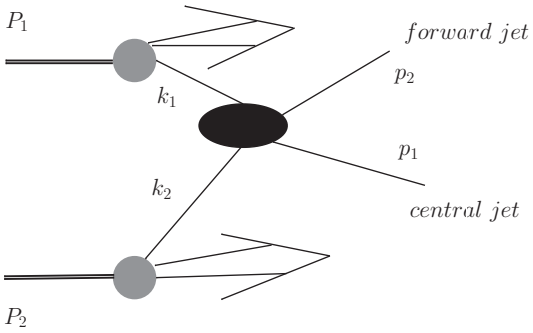

Figure 1: Jet production in the forward region in hadron-hadron collisions.

In this study we focus on the asymmetric configuration with one jet produced in the forward and the other in the central rapidity region as illustrated in Fig. 1. The fractions of the longitudinal momenta of the initial state partons are related to the transverse momenta and rapidities of the final state partons by

$$x_1 = \frac{1}{\sqrt{S}}\left(p_{t1}e^{y_1} + p_{t2}e^{y_2}\right), \qquad x_2 = \frac{1}{\sqrt{S}}\left(p_{t1}e^{-y_1} + p_{t2}e^{-y_2}\right), \tag{2.3}$$

where S is the squared energy in the center of mass system of the incoming hadrons. Hence, our central-forward configuration corresponds to one of the x_is being small and the other one large.

The first study of such configurations in the p-p collisions was performed in [28–30] using the CASCADE Monte Carlo generator [31]. Assuming, without loss of generality, that $x_1 \simeq 1$ and $x_2 \ll 1$ we have

$$k_1^\mu = x_1 P_1^\mu, \tag{2.4}$$
$$k_2^\mu = x_2 P_2^\mu + k_t^\mu, \tag{2.5}$$

where we used the Sudakov decomposition of the initial partons' 4-momenta. Here $P_{1,2}^\mu$ are the 4-momenta of incoming hadrons, which, in the center of mass frame, take the form $P_{1,2}^\mu = \sqrt{\frac{s}{2}}(1,0,0,\pm 1)$ and $P_1 \cdot P_2 = \frac{1}{2}S$. The momentum of the off-shell parton satisfies $k_2^2 = k_t^2 \equiv -k^2$, where $k \equiv k_t \equiv |\mathbf{k}|$. This leads to the following form of the cross section

$$\frac{d\sigma}{dy_1 dy_2 d^2p_{1t} d^2p_{2t}} = \sum_{a,c,d} \frac{1}{16\pi^3 (x_1 x_2 S)^2} \mathcal{M}_{ag\to cd} x_1 f_{a/A}(x_1,\mu^2)\, \phi_{g/B}(x_2,k^2,\mu^2) \frac{1}{1+\delta_{cd}}, \tag{2.6}$$

and

$$k^2 = p_{t1}^2 + p_{t2}^2 + 2p_{t1}p_{t2}\cos\Delta\phi, \tag{2.7}$$

where $\Delta\phi = \phi_1 - \phi_2$ is the azimuthal distance between the outgoing partons and $\mathcal{M}_{ag\to cd}$ is the matrix element for the $2 \to 2$ process with one off-shell initial state gluon and three on-shell partons, a, c, d, which can be either quarks or gluons [32]. The following partonic sub-processes contribute to the production of our dijet system

$$qg \to qg, \qquad gg \to q\bar{q}, \qquad gg \to gg. \tag{2.8}$$

On the side of the off-shell gluon in Eq. (2.6), we have the unintegrated gluon density $\phi_{g/B}(x_2, k^2\mu^2)$, which depends on the longitudinal momentum fraction x_2, on the transverse momentum of the off-shell gluon, and in general as well as on hard scale μ. The hard scale dependence introduces DGLAP-like ordering effects in the high energy factorization framework and makes it applicable in studies of exclusive final states. In our calculations, however, we follow the KMS [41]

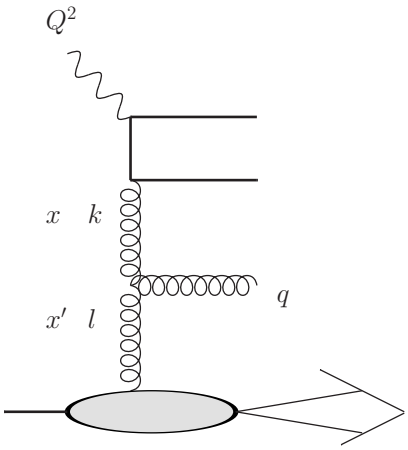

Figure 2: Diagrammatic representation of the F_2 structure function in *high energy factorization*.

scheme to introduce corrections to the gluon density which make it applicable to the studies of jet physics. Because of this we shall skip the argument μ in the expressions for the unintegrated gluon density below.

On the side of the on-shell parton, which is probed at high values of the longitudinal momentum fraction x_1, it is legitimate to use the collinear parton density $f_{a/A}(x_1, \mu^2)$.

The above result depends only on the difference of the azimuthal angles $\Delta\phi$, so one can change variables and integrate out one of angles ϕ_i. This leads to

$$\frac{d\sigma}{dy_1 dy_2 dp_{1t} dp_{2t} d\Delta\phi} = \sum_{a,c,d} \frac{p_{t1} p_{t2}}{8\pi^2 (x_1 x_2 S)^2} \mathcal{M}_{ag\to cd} x_1 f_{a/A}(x_1, \mu^2)\, \phi_{g/B}(x_2, k^2) \frac{1}{1+\delta_{cd}}\,, \qquad (2.9)$$

with $k^2 = p_{t1}^2 + p_{t2}^2 + 2p_{t1}p_{t2}\cos\Delta\phi$.

3 Unintegrated gluon density from the unified BK/DGLAP framework fitted to combined HERA data

The formulation of the NLO BFKL equation [33–35] has been known already for some time. Also the NLO BK equation has been derived [36] but, because of its complicated structure, only solutions of some approximate forms of the BK equations are known (see [37–40]). The basic formulation of the NLO BFKL equation is unstable (due to non-positive definite kernel) and in order to stabilize it one needs to resume a subset of higher order corrections [17, 18, 41]. In our study, we will use the approach to this problem formulated in [41] in which large part of the higher order corrections is provided by the consistency constraint on emissions of real gluons. The other important corrections are coming from running of the coupling constant and the nonsingular pieces of the DGLAP splitting functions. Other approaches were discusses in [42–44].

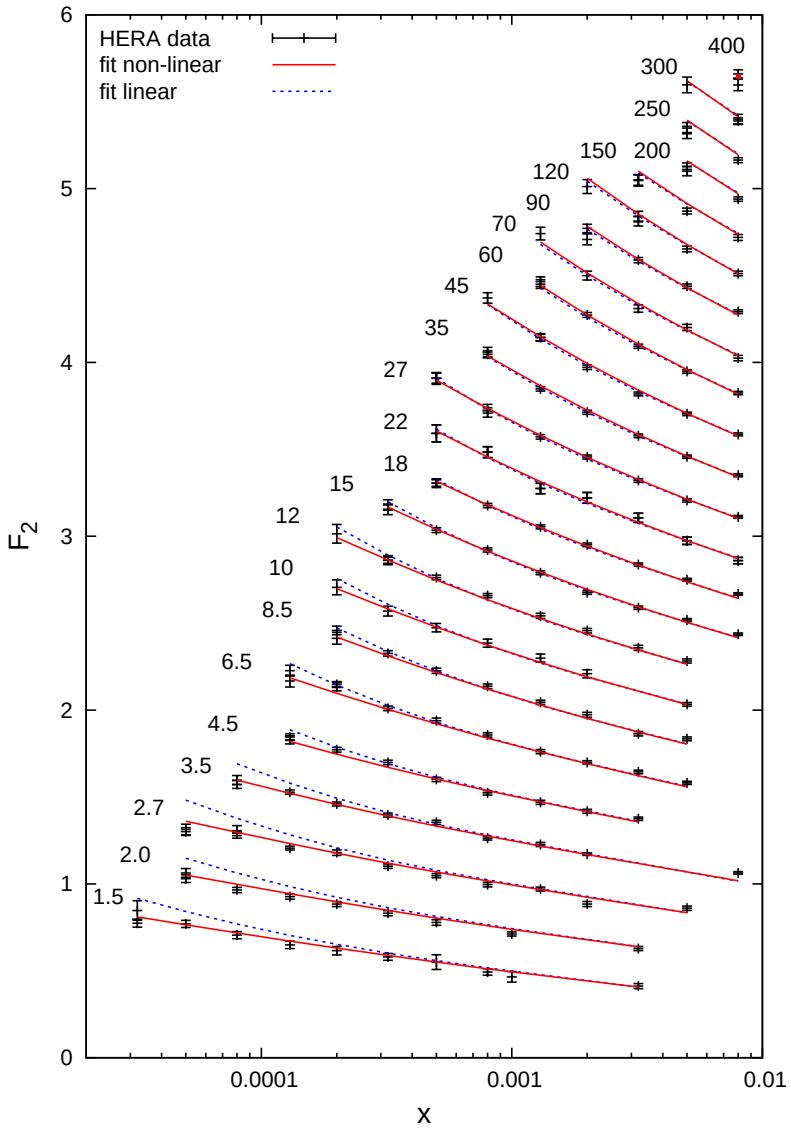

Figure 3: The proton structure function $F_2(x, Q^2)$ from the fit of our framework, in its linear and nonlinear variant, to the combined data from HERA [26] as a function of x for the Q^2 range from 1.5 to 400 GeV^2 (with the vertical offsets of 0.2).

The corresponding equation for the unintegrated gluon density reads [27, 45]

$$\begin{aligned}
\phi_p(x,k^2) \;=\; & \phi_p^{(0)}(x,k^2) \\
& + \frac{\alpha_s(k^2) N_c}{\pi} \int_x^1 \frac{dz}{z} \int_{k_0^2}^{\infty} \frac{dl^2}{l^2} \left\{ \frac{l^2 \phi_p(\frac{x}{z}, l^2)\, \theta(\frac{k^2}{z} - l^2) \;-\; k^2 \phi_p(\frac{x}{z}, k^2)}{|l^2 - k^2|} + \frac{k^2 \phi_p(\frac{x}{z}, k^2)}{|4l^4 + k^4|^{\frac{1}{2}}} \right\} \\
& + \frac{\alpha_s(k^2)}{2\pi k^2} \int_x^1 dz \left[\left(P_{gg}(z) - \frac{2N_c}{z} \right) \int_{k_0^2}^{k^2} dl^2\, \phi_p\left(\frac{x}{z}, l^2\right) + z P_{gq}(z) \Sigma\left(\frac{x}{z}, k^2\right) \right] \\
& - \frac{2\alpha_s^2(k^2)}{R^2} \left[\left(\int_{k^2}^{\infty} \frac{dl^2}{l^2} \phi_p(x, l^2) \right)^2 + \phi_p(x,k^2) \int_{k^2}^{\infty} \frac{dl^2}{l^2} \ln\left(\frac{l^2}{k^2}\right) \phi_p(x, l^2) \right] , \qquad (3.1)
\end{aligned}$$

where $z = x/x'$ (see Fig. 2 for explanation of the variables). For convenience, we omit the g subscript in the unintegrated gluon density symbol and keep only the subscript denoting the

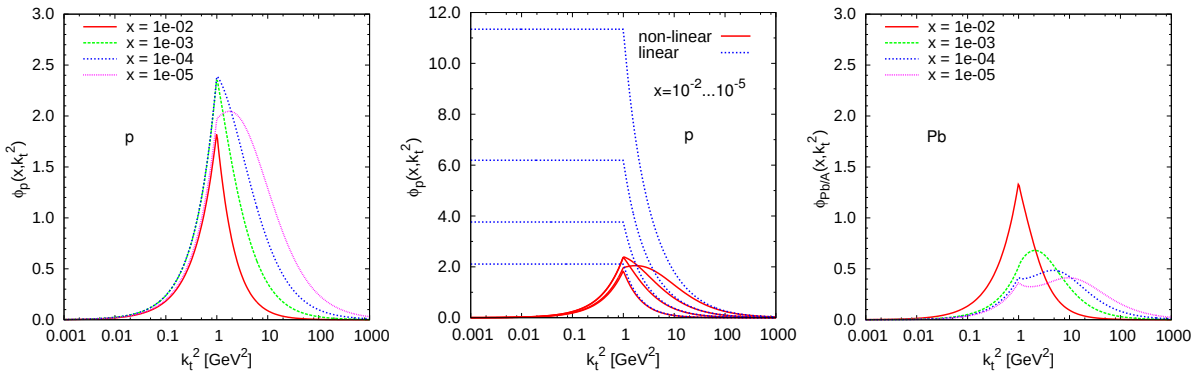

Figure 4: Left: Unintegrated gluon density in the proton from the solution of Eq. (3.1) with free parameters fitted to F_2 data. Middle: Comparison of the gluon density from the left plot with the unintegrated gluon from the fit using only the linear part of Eq. (3.1). Right: Unintegrated gluon density in the Pb nucleus obtained as for the proton case but with the nonlinear term in Eq. (3.1) enhanced by $A^{1/3}$ with $A = 207$.

hadron. The theta function in Eq. (3.1) introduces the kinematical constraint and the nonlinear term, which supplies unitarity corrections, is given by the triple pomeron vertex [46]. The two terms in the third line in Eq. (3.1) correspond to the DGLAP effects generated by that part of the splitting function $P_{gg}(z)$ which is nonsingular in the limit $z \to 0$ and by the quarks respectively, with $\Sigma(x, k^2)$ corresponding to the singlet quark distributions. The At LO in $\ln 1/x$ this equation reduces to the BK equation, after performing Fourier transform to the coordinate space [13, 27, 46, 47]. For numerical method to solve Eq. (3.1) we refer the reader to [27].

The strength of the nonlinear term in Eq. (3.1) is controlled by the parameter R which has an interpretation of the proton radius and it comes from integration of the gluon density over the impact parameter b. In our framework, we assume the uniform distributions of gluons in the nucleon therefore our gluon density is proportional to $\Theta(R - b)$ [27].

The input gluon distribution $\phi_p^{(0)}(x, k^2)$ is is given by

$$\phi_p^{(0)}(x, k^2) = \frac{\alpha_S(k^2)}{2\pi k^2} \int_x^1 dz P_{gg}(z) \frac{x}{z} g\left(\frac{x}{z}, k_0^2\right) , \tag{3.2}$$

where $xg(x, k_0^2)$ is the integrated gluon distribution at the initial scale, which we set to $k_0^2 = 1\,\mathrm{GeV}^2$, and we take the following parametrization

$$xg(x) = N(1 - x)^\beta (1 - Dx) , \tag{3.3}$$

which is similar to what was used in [48]. For the strong coupling, we take the one-loop result with Λ_{QCD} set to 350 MeV.

The evolution equation (3.1) is used to determine the unintegrated gluon above the initial momentum scale that is for $k^2 > 1\,\mathrm{GeV}^2$. In the region $k^2 < 1\,\mathrm{GeV}^2$, the gluon density $\phi_p(x, k^2)$ is constrained by the condition that it should match the evolved unintegrated gluon density at $k^2 = k_0^2$. We choose to parametrize the unintegrated gluon in this region by

$$\phi_p(x, k^2) = k^2 \phi_p(x, k_0^2 = 1\,\mathrm{GeV}^2) \qquad \text{for} \quad k^2 < 1\,\mathrm{GeV}^2 , \tag{3.4}$$

which is motivated by the shape of the gluon density obtained from solution of the LO BK equation in the saturated regime [49].

The unintegrated gluon density from Eqs.(3.1)–(3.3) convoluted with impact factors taken from [41] allows one to compute the structure function $F_2(x, Q^2)$, which in turn can be used to

fit the free parameters of the model. We performed such a fit to the combined HERA data [26] in the kinematical range of $x < 0.01$ and the full range of Q^2. As shown in Fig. 3 (red solid line), we obtain a very good description of data, which corresponds to $\chi^2/\text{ndof} = 1.73$ and the following values of the parameters: $N = 0.994$, $\beta = 18.6$, $D = -82.1$ and $R = 2.40\,\text{GeV}^{-1}$.

In Fig. 4 (left) we show the unintegrated gluon density, corresponding to the above fit, as a function of the transverse momentum of the gluon for a range of x values. The gluon from the evolution is sewed at $k^2 = 1\,\text{GeV}^2$ with the parametrization (3.4). The sharp peek corresponds to the point in k where the matching was done. We see however that as one goes to lower x values, perturbatively generated maximum starts to emerge. That is a signal of the presence of saturation scale defining the most probable momentum of the gluon. The results for estimated value of the saturation scale are in an agreement with [40, 49, 50]

Our main focus in this study is on the framework with saturation of gluon density described above which is based on the nonlinear evolution equation (3.1). It is however interesting to compare our results to the case in which the gluon is determined from the framework without saturation. This is naturally provided by the linear version of Eq. (3.1) that corresponds to dropping the last term on the right hand side of that equation, which now becomes independent of R. We performed an analogous fit to the one described above but taking the linearized version of Eq. (3.1) and restricting Q^2 to the values above $4.5\,\text{GeV}^2$ to stay outside of the region where the saturation effects may be important. The fit parameters at the minimal value of $\chi^2 = 1.51$ are: $N = 0.004$, $\beta = 26.7$ and $D = -51102$. The corresponding results are shown in Fig. 3 (blue dashed line) for the whole range of Q^2 including the bins below $4.5\,\text{GeV}^2$, which were not used in the fit. We see that the linear gluon gives too strong rise of F_2 with x especially at low values of Q^2. This remains true even if we fit the linear version of Eq. (3.1) to the full range of Q^2. The best value of χ^2 we were able to achieve in this case was 3.86. We therefore conclude that some mechanism damping the gluon density at low x and low Q^2 is necessary to describe the F_2 HERA data in the full range of Q^2. This mechanism corresponds to saturation of gluon density.

We summarize this part of our study by comparing the two versions of the unintegrated gluon density, linear and non-linear, in Fig. 4 (middle). The linear gluon for $k^2 > 1\,\text{GeV}^2$ corresponds to the fit described above. For the values of k^2 below $1\,\text{GeV}^2$, similarly to what we did for the non-linear case, we parametrize our gluon, this time by $\phi(x, k^2) = \phi(x, k_0^2 = 1\,\text{GeV}^2)$. We see in Fig. 4 (middle) that at large values of x and k_t, both distributions are similar. As one goes to lower k_t, however, the linear gluon rises much faster than the non-linear one. This effect becomes significantly stronger for smaller values of x.

4 Central-forward dijet production in p-p collisions at the LHC

We are now in the position to compute the cross section for central-forward jet production in the proton-proton collision. We use directly the formula (2.9) with the matrix element calculated in [32] and the unintegrated gluon distributions determined in the previous section. For the collinear parton distributions we take CTEQ6mE [51].

The CMS collaboration has reported the measurement [52] of the transverse momentum distributions of pairs of jets, one of which is restricted to be in the forward and the other in the central part of the detector. This measurement has already been confronted with various Monte Carlo predictions including HEJ [53, 54] and CASCADE [31]. We compute the corresponding distributions in our framework taking the selection cuts which match those of CMS. We set the normalization and factorization scale equal to the fixed value of 60 GeV and vary it by the factors 1/2 and 2 to asses the uncertainty.

The results for jet p_t spectra are shown in Fig. 5 for the central (left) and the forward (right) jet respectively. We find that our predictions based on nonlinear (red) and linear (green) evolu-

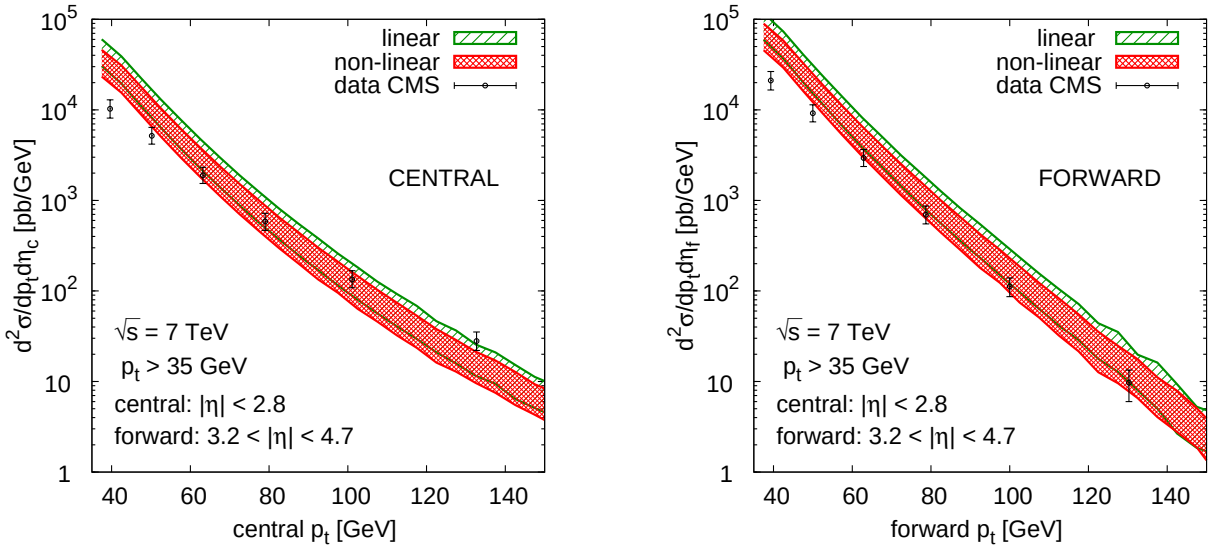

Figure 5: The transverse momentum spectra of the central (left) and forward (right) jets from our framework compared to the CMS data. The uncertainty bands come from varying the factorization and renormalization scale by factor two around the central value of $\mu = 60\,\mathrm{GeV}$.

tion equations reproduce the pattern of the CMS measurement. As expected, this observable in experimentally accessible region is weakly sensitive to saturation. We see some suppression of the cross section based on the nonlinear evolution equation which is a manifestation of the lower gluon density in the small k_t region. The description with both densities is good despite the fact that our modeling of jets is very simple since, in the framework we use here, each of the two jets is just a single parton. Moreover, the small excess of low-p_t is expected precisely because of that. Adding a parton shower on the top of our partonic result would cause some energy to go out of the jet and that would affect the low-p_t jets since they are broader then the high-p_t jets. For related discussion within the HEJ approach see [54, 55]. Similarly, we may expect that due to large rapidity gap between the produced jet, some extra BFKL-type radiation could be emitted. An explicit demonstration of the role of these effects in our framework opens an interesting possibility for future work. However, they are not crucial for the following discussion since they will affect the results for p-p and p-Pb in the same way and our focus in this work is on the relative differences between this two cases.

Also the slightly smaller cross section in the high-p_t region for the central jet is well understood. As follows from Eq. (2.3), the value of x_2 probed by the central jet $p_t \sim 140\,\mathrm{GeV}$ corresponds to $x_2 \sim 0.02$ which is beyond the limit we used in our fits of unintegrated gluon and therefore our predictive power in this region is limited. We have checked that if the gluon is fitted with the upper limit on x extended to 0.02, the result for p_t distribution of the central jet becomes consistent with the data also in the high-p_t region. Trying to extend our framework to higher values of x would be in itself an interesting project. It goes however beyond the scope of this paper, therefore throughout this study, we restrict ourselves to the region of $x < 0.01$. It should be emphasized, that even without going to large values of x the distributions from Fig. 5 are unique since they give direct access to the unintegrated gluon at medium and large values of k_t, provided that one works in the framework which permits to compute gluon in that region. The framework we adopted for this study satisfies that criterion. That opens the possibility to study the importance of terms of higher order from the point of view of BFKL, i.e. energy conservation and subleading pieces of the splitting function.

5 Signatures of saturation in central-forward dijet production in p-Pb collisions

In the preceding sections, we have shown that the *high energy factorization* formalism with the unintegrated gluon from the QCD evolution equation with saturation can successfully account for the features measured both in the e-p and p-p collisions. The slightly less precise description of the data in the latter case is expected and fully understood, and it can be traced back to the purely partonic nature of our result or to the upper limit on the x used in our fits of unintegrated gluon.

One of the main features of the formalism we use is that the unintegrated gluon is determined from the nonlinear evolution equation and therefore it exhibits saturation effects around certain momentum scale $Q_s(x)$. In this section, we address the question whether those effects could be studied experimentally in collisions at the LHC.

The main challenge of such a study, as pointed out by numerous analysis of HERA data [40, 56–59], is that the saturation scale in the proton seems to be of the order of a few GeV, hence it lies just at the border between perturbative and non-perturbative regime of QCD. This makes it difficult to access both theoretically and experimentally. One way to improve the situation is to go to the p-A collisions since, as widely discussed in the literature, the saturation scale in the nucleus is expected to be significantly higher than in the proton [3, 6, 60–62]. To estimate the possible effects of saturation in the heavy nucleus we use a simple formula for the nucleus radius following from counting the number of nucleons for Woods-Saxon nuclear density profile. The radius of the nucleus reads

$$R_{\rm A} = R\, A^{1/3}\,, \tag{5.1}$$

where R is the proton radius, which is one of the fitted parameters of our framework as described in section 3 and A is the mass number ($A = 207$ for Pb, $A = 196$ for Au). The above definition has the property that in the limit $A \to 1$ the result for the proton is recovered.

Analogous equation to Eq. (3.1) for the Heavy Ion (HI) normalized to the proton reads

$$\begin{aligned}
\phi_{\rm HI/A}(x,k^2) \;&=\; \phi^{(0)}_{\rm HI/A}(x,k^2) \\
&+ \frac{\alpha_s(k^2)N_c}{\pi}\int_x^1 \frac{dz}{z}\int_{k_0^2}^{\infty}\frac{dl^2}{l^2}\left\{\frac{l^2\phi_{\rm HI/A}(\frac{x}{z},l^2)\,\theta(\frac{k^2}{z}-l^2)\;-\;k^2\phi_{\rm HI/A}(\frac{x}{z},k^2)}{|l^2-k^2|}+\frac{k^2\phi_{\rm HI/A}(\frac{x}{z},k^2)}{|4l^4+k^4|^{\frac{1}{2}}}\right\} \\
&+ \frac{\alpha_s(k^2)}{2\pi k^2}\int_x^1 dz\left[\left(P_{gg}(z)-\frac{2N_c}{z}\right)\int_{k_0^2}^{k^2} dl^2\,\phi_{\rm HI/A}\left(\frac{x}{z},l^2\right)+zP_{gq}(z)\Sigma_{HI/A}\left(\frac{x}{z},k^2\right)\right] \\
&- \frac{2A^{1/3}\alpha_s^2(k^2)}{R^2}\left[\left(\int_{k^2}^{\infty}\frac{dl^2}{l^2}\phi_{\rm HI/A}(x,l^2)\right)^2+\phi_{\rm HI/A}(x,k^2)\int_{k^2}^{\infty}\frac{dl^2}{l^2}\ln\left(\frac{l^2}{k^2}\right)\phi_{\rm HI/A}(x,l^2)\right]\,,
\end{aligned} \tag{5.2}$$

where we used Eq. (5.1) to express the radius of the heavy ion in terms of the proton radius thus $\phi_{\rm HI}(x,k^2) \equiv A\phi_{\rm HI/A}(x,k^2)$ is the distribution of gluons per nucleon in the nucleus. We see that the strength of the nonlinear term in Eq. (5.2) is enhanced by $A^{1/3}$ [6, 63]. We are aware that this modification is not sufficient to fully model the nuclear target and is a somewhat crude approximations but it will suffice as a first approximation to estimate the saturation effects in the nucleus. For a more sophisticated approach see [64] and references therein.

In Fig. 4 (right) we show the gluon density in the Pb nucleus which results from the application of the above prescription to the unintegrated gluon distribution in the proton from Fig. 4 (left). We notice that due to stronger saturation effects in Pb, the gluon density is lower than that in the proton for the same value of x. We also see that in Pb the maxima are shifted towards larger values of the gluon's transverse momentum k_t, which corresponds to the larger saturation scale in the nucleus.

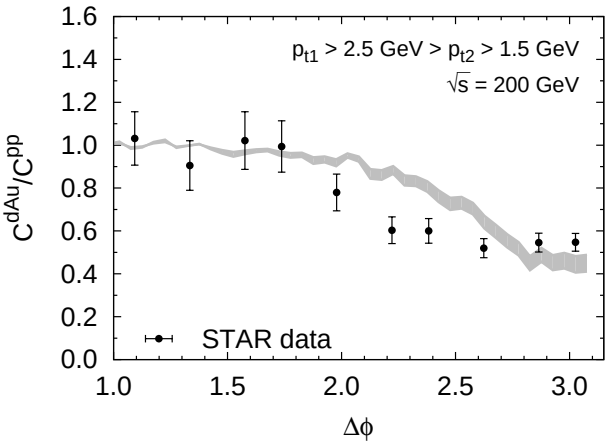

Figure 6: Ratio of d-Au/p-p coincidence probabilities $C(\Delta\phi)$ for the forward dihadron production at RHIC as a function of the azimuthal distance between the particles. The d-Au data were shifted by a constant. The errors of the ratio were determined from relative errors of each $C(\Delta\phi)$ before the shift. The band corresponds to our prediction with the uncertainty related the unknown yield of uncorrelated dihadron production.

An observable which is very well suited to study saturation is the azimuthal correlation of the central and forward jet. It is an inclusive observable that measures radiation between jets and is therefore sensitive to potential saturation effects which are supposed to decrease the rate of emissions when the parton density is probed at very low x where the high density of partons leads to their recombinations. The most interesting region of $\Delta\phi$ is that close to π since the produced jets are almost back to back and the gluon density is probed at low k_t.

Before we turn to the discussion of our main results for the central-forward dijets production at the LHC, it is interesting to check how the magnitude of the suppression of decorrelations predicted by our framework compares to the existing data for the forward dihadron production from RHIC. STAR and PHENIX measured the coincidence probability defined as the ratio of the yield of the π^0-pair to the inclusive π^0 yield, $C(\Delta\phi) = N^{\rm pair}(\Delta\phi)/N^{\rm incl}$. Precise determination of this observable requires convolution of our diparton pair from Eq. (2.9) with the fragmentation functions as well as computation of inclusive π^0 production and also the uncorrelated π^0 pair production (see [3, 61] for corresponding results in different frameworks). All this goes beyond the scope of the present paper and will be published elsewhere. Nevertheless, we can make a meaningful estimate for a related quantity that can be compared to the STAR data [65, 66]. To minimise the contribution from the uncorrelated pair production we shift the d+Au data by -0.00145, similarly to what has been done in [3], so that the d+Au and p-p data coincide below $\Delta\phi = \pi/2$. Assuming that the remaining yield comes predominantly from the correlated dihadron production, we compare the ratio $C^{\rm dAu}(\Delta\phi)/C^{\rm pp}(\Delta\phi)$ for the experimental data with that from our computation for diparton production at $\sqrt{s} = 200\,\text{GeV}$ with $p_{t1} > 2.5\,\text{GeV}$, $p_{t1} > p_{t2} > 1.5\,\text{GeV}$ and $2.4 < y_{1,2} < 4.0$. By using the above ratio we do not need to worry about the normalization to the inclusive spectra and it is also reasonable to expect that most of the effects from parton fragmentation will cancel. Our absolute prediction (with $\mu = p_{t1}$) for the ratio of the coincidence probabilities is shown in Fig. 6 together with the data from STAR [65,66]. Since our framework does not depend on the impact parameter, we chose to compare to the data averaged over centralities. The band in Fig. 6 corresponds to the uncertainty related to the assumption of negligible contribution form the uncorrelated production after the shift described above. To asses this uncertainty we considered an alternative scenario in which half of the yield seen in the data at $\Delta\phi = \pi/2$ is attributed to the independent production and the other half

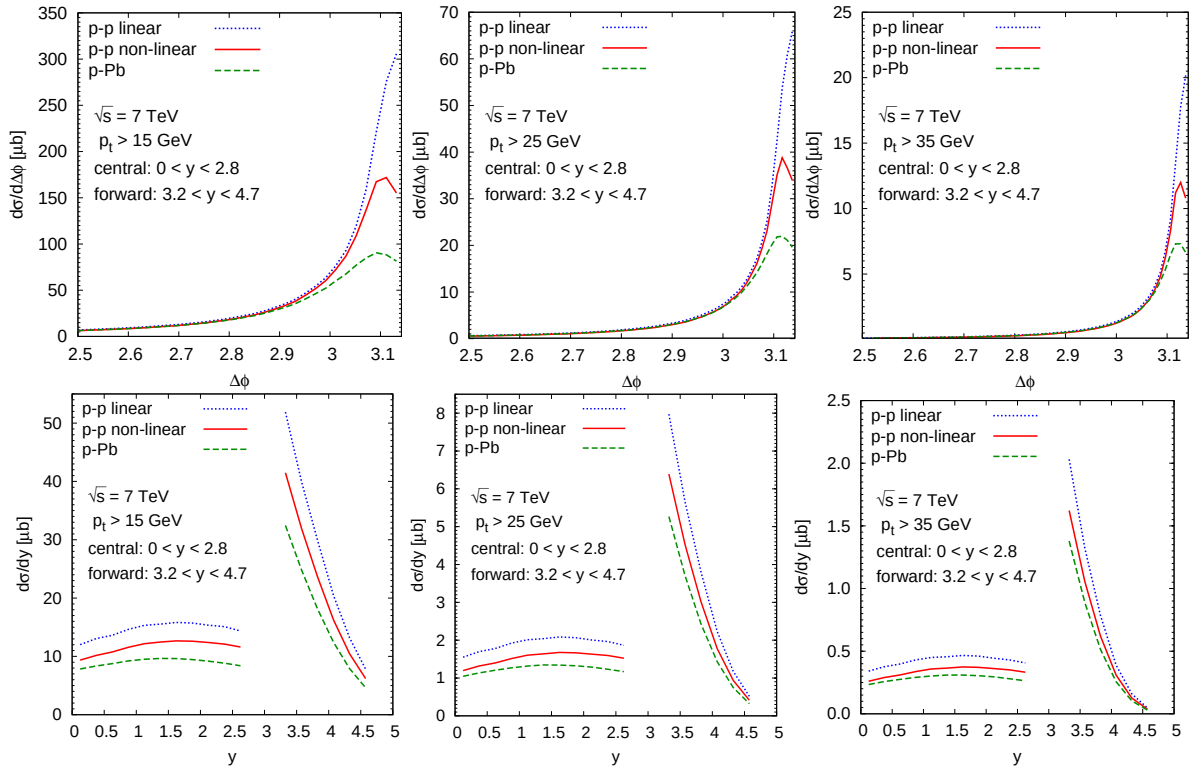

Figure 7: Differential cross sections for central-forward dijet production as functions of azimuthal distance between the jets $\Delta\phi$ (top) or rapidities of the jets (bottom) for the case of p-p and p-Pb collisions and three different cuts on jets' p_t.

to the correlated production that we can predict with our framework. As we see in Fig. 6, the suppression pattern of the away-side peak of the dihadron spectra from d-Au collisions at RHIC is correctly reproduced by our calculation which shows that our theoretical framework captures the essential physics of this class of processes.

We move now to the central-forward dijet production in the p-Pb collisions at the LHC. In the top row of Fig. 7 we show the differential cross section for the central-forward dijet production as a function of the azimuthal distance between the jets for the p-p and p-Pb collisions. To obtain those results we employed the linear and nonlinear versions of the evolution equation (3.1) for the proton and the evolution equation (5.2) for Pb. We used selection similar to that form the previous section except for the p_t cut which we now vary from 15, through 25, to 35 GeV and the rapidity which is restricted to positive values. The latter corresponds to the fact that, contrary to the p-p case, the p-Pb collision is asymmetric and, as follows from Eq. (2.3), one probes the gluon density in Pb at low x only by measuring the forward jets going into the region of positive rapidity.

First observation from Fig. 7 is that the non-linear evolution leads to a significant suppression of the $\Delta\phi$ and rapidity distributions already for the proton case. This alone is a clear manifestation of saturation. Then we see that the $\Delta\phi$ cross section near the peak region is suppressed further by the factor of about two for the case of the p-Pb collision and the effect extends to lower values of $\Delta\phi$ as we lower the p_t threshold (going from right to left plot). This is precisely the consequence of gluon saturation which is stronger in the Pb nucleus then in the proton and therefore the unintegrated gluon distribution in the region of small and medium k_t is suppressed in Pb compared to the proton case as shown in Fig. 4 (right). It is this region of gluon's k_t that is probed by the dijet configurations with $\Delta\phi \sim \pi$ and that is what leads to the lower cross section in the area of the peak.

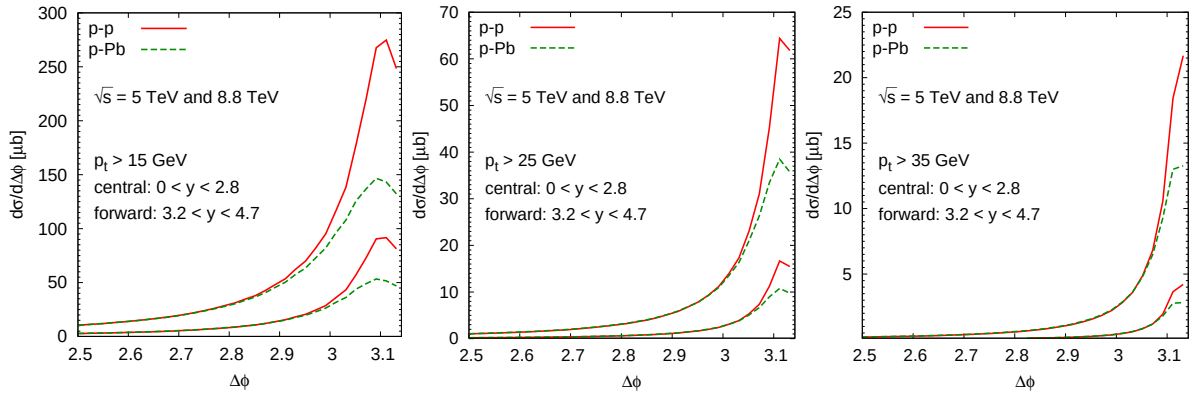

Figure 8: Differential cross sections for central-forward dijet production at $\sqrt{s} = 5$ TeV and 8.8 TeV as functions of azimuthal distance between the jets $\Delta\phi$ for the case of p-p and p-Pb collisions and three different cuts on jets' p_t.

We notice that the non-linear results have a dip structure near $\Delta\phi \simeq \pi$. This is a consequence of the feature of a high energy factorisable gluon density which goes down to zero like k^2. On the other hand, as discussed in section 3, in the linear case we model the behaviour of the unintegrated gluon density by assuming that the gluon density behaves like a constant and therefore the linear result for the $\Delta\phi$ distribution keeps growing as $\Delta\phi \to \pi$. These features make the $\Delta\phi$ distribution a particularly interesting observable for testing shapes of gluon densities and more generally the validity of the high energy factorization as pointed out recently in [67]. On the top of that, the region near $\Delta\phi \simeq \pi$ is also sensitive to Sudakov (virtual corrections) and parton shower effects (taking energy from the jets we measure) which have the tendency to reduce the cross section in the region $\Delta\phi$ near the peak. Some refinement along those lines could be envisaged in the future. These effects act however in a similar way for the proton and for the heavy ion since they affect the hard scattering. Because we are interested in searching for saturation effects in the initial state parton density, it is legitimate to neglect them in this study and focus on the relative difference between the cases of p-p and p-Pb collisions. The main point we would like to emphasize here is that the suppression due to saturation predicted in Fig. 7 is both strong and it extends for large enough range in $\Delta\phi$ to allow for experimental discrimination between the linear and non-linear scenario, even if the very small region near $\Delta\phi = \pi$ may profit from further refinements.

In the bottom row of Fig. 7 we present the rapidity distributions of forward and central jets for the case of p-p and p-Pb collisions. As expected, the saturation effects which are stronger in the nucleus than in the proton lead to lower yields both for the central and forward jet production in the p-Pb collision. Consistently with the decorrelation results, also here, the difference between p-p and p-Pb becomes more pronounced as one lowers the value of the jet p_t cut.

Finally, in Fig. 8 we show decorrelations plots similar to those from Fig. 7 but for the energies of the actual p-Pb collisions, i.e. the current $\sqrt{s} = 5\,\text{TeV}$ and the nominal $\sqrt{s} = 8.8\,\text{TeV}$. As expected, the total yields increase with energy but the relative difference between the p-p and p-Pb case seems to remain similar.

6 Conclusion and outlook

We presented the analysis of e-p, p-p and p-Pb collisions in the framework of high energy factorisation with the unintegrated gluon density given by the nonlinear QCD evolution equation. We have shown that this formalism can successfully account for features measured in e-p and

p-p data. For comparison, we also performed calculations within the linear evolution framework and discussed differences between results from the two scenarios.

We then used the above non-linear framework to provide an estimate of the effects of gluon saturation in the nuclei. We presented predictions for the azimuthal decorrelations as well as the rapidity distributions for the p-p and p-Pb collisions. Our main finding is that saturation in the Pb nucleus has a potential to manifest itself as a factor two suppression of the central-forward jet decorrelation in the region of the azimuthal distance between the jets $\Delta\phi \sim \pi$. The effect becomes more pronounced with lower cuts on jets' transverse momenta.

The framework used in our study allows for a number of refinements that would lead to a better description of data as well as for more accurate predictions. We could, for example, extend our analysis by introducing non-trivial impact parameter dependence of the unintegrated gluon density. That would allow us to study saturation effects as a function of centrality of the p-Pb collision.

Another interesting possibility for future work is opened by an ongoing discussion on breakdown of the high energy factorization and related issue of multiple definitions of the unintegrated gluon density. As advocated in [68, 69], this generalized description provides a framework which is better theoretically motivated. There are two reasons why the study in such a framework would be interesting. First of all, because that framework was derived only with simplified matrix elements, whereas in our study we have the exact ones. That would allow one to investigate the relative importance of the corrections to the high energy factorization formula from section 2 compared to the case with exact kinematics. The second reason is that the consensus as to which gluon distribution should be used to study dijet production has not been reached yet. The definition of the unintegrated gluon that we used in this study follows directly from Feynman diagrams and, as argued in [70], is therefore the valid form of unintegrated gluon density. Hence, we performed our study in the framework of the high energy factorization and the results from sections 4 and 5 can then be used in the future as a benchmark for further studies within extended formalisms.

Finally, we note that the approach used in this study is unique as it allows one to study hard final states in the framework with saturation. This offers the possibility to constrain the unintegrated gluon density in the large range of momentum available at the LHC. Our current limit of $x < 0.01$ could be extended to higher values of x by using the gluon density from the CCFM equation with saturation [71]. That would allow for a better description of the high p_t tail of jet spectra.

Acknowledgments

We would like to thank Krzysztof Golec-Biernat for thorough reading of this manuscript and for numerous valuable suggestions. We acknowledge useful correspondence with Jeppe R. Andersen regarding the dijet spectra. We acknowledge correspondence with Hannes Jung and Maciej Misiura regarding the FSR effects on dijet spectra. We appreciate valuable discussions and correspondence with David d'Enterria, Grzegorz Brona, Michal Deak, Francesco Hautmann, Cyrille Marquet, Andreas van Hameren, Hannes Jung and Pierre van Mehelen, Bowen Xiao. During this research KK was supported by the Foundation for Polish Science with the grant Homing Plus/2010-2/6. SS acknowledges the Foundation for Polish Science for support of his stay in Instytut Fizyki Jądrowej PAN during realization of this project.

References

[1] L. V. Gribov, E. M. Levin and M. G. Ryskin, Phys. Rept. **100** (1983) 1.

[2] A. M. Stasto, K. J. Golec-Biernat, J. Kwiecinski, Phys. Rev. Lett. **86** (2001) 596-599.

[3] J. L. Albacete, C. Marquet, Phys. Rev. Lett. **105** (2010) 162301.

[4] A. Dumitru, K. Dusling, F. Gelis *et al.*, Phys. Lett. **B697** (2011) 21-25.

[5] J. L. Albacete, J. G. Milhano, P. Quiroga-Arias and J. Rojo, arXiv:1203.1043 [hep-ph].

[6] F. Gelis, E. Iancu, J. Jalilian-Marian and R. Venugopalan, Ann. Rev. Nucl. Part. Sci. **60** (2010) 463 [arXiv:1002.0333 [hep-ph]].

[7] T. Sjostrand, S. Mrenna and P. Z. Skands, JHEP **0605** (2006) 026 [hep-ph/0603175].

[8] S. Catani, M. Ciafaloni, F. Hautmann, Nucl. Phys. **B366** (1991) 135-188.

[9] E. A. Kuraev, L. N. Lipatov and V. S. Fadin, Sov. Phys. JETP **45**, 199 (1977) [Zh. Eksp. Teor. Fiz. **72**, 377 (1977)].

[10] I. I. Balitsky and L. N. Lipatov, Sov. J. Nucl. Phys. **28**, 822 (1978) [Yad. Fiz. **28**, 1597 (1978)].

[11] I. Balitsky, Nucl. Phys. **B463** (1996) 99-160.

[12] Y. V. Kovchegov, Phys. Rev. D **60** (1999) 034008.

[13] Y. V. Kovchegov, Phys. Rev. D **61** (2000) 074018.

[14] M. Ciafaloni, Nucl. Phys. B **296**, 49 (1988).

[15] S. Catani, F. Fiorani and G. Marchesini, Nucl. Phys. B **336**, 18 (1990).

[16] S. Catani, F. Fiorani and G. Marchesini, Phys. Lett. B **234**, 339 (1990).

[17] G. P. Salam, JHEP **9807** (1998) 019 [hep-ph/9806482].

[18] M. Ciafaloni and D. Colferai, Phys. Lett. B **452** (1999) 372 [hep-ph/9812366].

[19] M. Ciafaloni, D. Colferai, G. P. Salam and A. M. Stasto, Phys. Lett. B **587** (2004) 87 [hep-ph/0311325].

[20] K. Kutak, Phys. Lett. B **675** (2009) 332 [arXiv:0903.3521 [hep-ph]].

[21] Y. V. Kovchegov, Nucl. Phys. A **854** (2011) 3 [arXiv:1007.5021 [hep-ph]].

[22] C. Marquet and R. B. Peschanski, Phys. Lett. B **587** (2004) 201 [arXiv:hep-ph/0312261].

[23] D. G. d'Enterria, Eur. Phys. J. A **31** (2007) 816.

[24] E. Iancu, C. Marquet and G. Soyez, Nucl. Phys. A **780** (2006) 52.

[25] J. R. Andersen and A. Sabio Vera, Phys. Lett. B **567** (2003) 116.

[26] F. D. Aaron *et al.* [H1 and ZEUS Collaboration], JHEP **1001** (2010) 109 [arXiv:0911.0884 [hep-ex]].

[27] K. Kutak and J. Kwiecinski, Eur. Phys. J. C **29** (2003) 521 [arXiv:hep-ph/0303209].

[28] M. Deak, F. Hautmann, H. Jung and K. Kutak, arXiv:1012.6037 [hep-ph].

[29] M. Deak, F. Hautmann, H. Jung and K. Kutak, arXiv:0908.1870 [hep-ph].

[30] M. Deak, F. Hautmann, H. Jung and K. Kutak, Eur. Phys. J. C **72** (2012) 1982 [arXiv:1112.6354 [hep-ph]].

[31] H. Jung, S. Baranov, M. Deak, A. Grebenyuk, F. Hautmann, M. Hentschinski, A. Knutsson and M. Kramer *et al.*, Eur. Phys. J. C **70** (2010) 1237.

[32] M. Deak, F. Hautmann, H. Jung and K. Kutak, JHEP **0909** (2009) 121 [arXiv:0908.0538 [hep-ph]].

[33] V. S. Fadin, M. I. Kotsky and L. N. Lipatov, hep-ph/9704267.

[34] V. S. Fadin, R. Fiore, A. Flachi and M. I. Kotsky, Phys. Lett. B **422** (1998) 287 [hep-ph/9711427].

[35] V. S. Fadin and L. N. Lipatov, Phys. Lett. B **429** (1998) 127 [hep-ph/9802290].

[36] I. Balitsky and G. A. Chirilli, Phys. Rev. D **77** (2008) 014019 [arXiv:0710.4330 [hep-ph]].

[37] D. N. Triantafyllopoulos, Nucl. Phys. B **648** (2003) 293 [arXiv:hep-ph/0209121].

[38] R. B. Peschanski and S. Sapeta, Phys. Rev. D **74** (2006) 114021 [arXiv:hep-ph/0610354].

[39] R. Enberg, Phys. Rev. D **75** (2007) 014012 [arXiv:hep-ph/0612005].

[40] J. L. Albacete, N. Armesto, J. G. Milhano, P. Quiroga-Arias and C. A. Salgado, Eur. Phys. J. C **71** (2011) 1705 [arXiv:1012.4408 [hep-ph]].

[41] J. Kwiecinski, A. D. Martin and A. M. Stasto, Phys. Rev. D **56** (1997) 3991 [arXiv:hep-ph/9703445].

[42] H. Kowalski, L. N. Lipatov, D. A. Ross and G. Watt, Eur. Phys. J. C **70** (2010) 983 [arXiv:1005.0355 [hep-ph]].

[43] A. Sabio Vera, Nucl. Phys. B **722** (2005) 65 [hep-ph/0505128].

[44] E. Gotsman, E. Levin, M. Lublinsky and U. Maor, Eur. Phys. J. C **27** (2003) 411 [hep-ph/0209074].

[45] K. Kutak and A. M. Stasto, Eur. Phys. J. C **41** (2005) 343 [arXiv:hep-ph/0408117].

[46] J. Bartels and M. Wusthoff, Z. Phys. C **66** (1995) 157.

[47] J. Bartels and K. Kutak, Eur. Phys. J. C **53** (2008) 533.

[48] A. Bacchetta, H. Jung, A. Knutsson, K. Kutak and F. Samson-Himmelstjerna, Eur. Phys. J. C **70** (2010) 503 [arXiv:1001.4675 [hep-ph]].

[49] S. Bondarenko, Phys. Lett. B **665** (2008) 72 [arXiv:0802.1802 [hep-ph]].

[50] C. Marquet and C. Royon, Nucl. Phys. B **739** (2006) 131 [hep-ph/0510266].

[51] J. Pumplin, D. R. Stump, J. Huston, H. L. Lai, P. M. Nadolsky and W. K. Tung, JHEP **0207** (2002) 012 [arXiv:hep-ph/0201195].

[52] CMS Collaboration, " Cross section measurement for simultaneous production of a central and a forward jet in proton-proton collisions at sqrt(s)=7 TeV," CMS-PAS-FWD-10-006 (2011).

[53] J. R. Andersen and J. M. Smillie, JHEP **1001** (2010) 039 [arXiv:0908.2786 [hep-ph]].

[54] J. R. Andersen and J. M. Smillie, JHEP **1106** (2011) 010 [arXiv:1101.5394 [hep-ph]].

[55] J. R. Andersen, L. Lonnblad and J. M. Smillie, JHEP **1107** (2011) 110 [arXiv:1104.1316 [hep-ph]].

[56] K. J. Golec-Biernat and M. Wusthoff, Phys. Rev. D **59** (1998) 014017 [hep-ph/9807513].

[57] H. Kowalski and D. Teaney, Phys. Rev. D **68** (2003) 114005 [hep-ph/0304189].

[58] J. Bartels, K. J. Golec-Biernat and H. Kowalski, Phys. Rev. D **66** (2002) 014001 [hep-ph/0203258].

[59] E. Iancu, K. Itakura and S. Munier, Phys. Lett. B **590** (2004) 199 [hep-ph/0310338].

[60] F. Dominguez, D. E. Kharzeev, E. M. Levin, A. H. Mueller and K. Tuchin, Phys. Lett. B **710** (2012) 182 [arXiv:1109.1250 [hep-ph]].

[61] A. Stasto, B. -W. Xiao and F. Yuan, arXiv:1109.1817 [hep-ph].

[62] K. Tuchin, Nucl. Phys. A **846** (2010) 83 [arXiv:0912.5479 [hep-ph]].

[63] J. Jalilian-Marian and Y. V. Kovchegov, Prog. Part. Nucl. Phys. **56** (2006) 104 [hep-ph/0505052].

[64] B. Schenke, P. Tribedy and R. Venugopalan, arXiv:1202.6646 [nucl-th].

[65] E. Braidot [STAR Collaboration], arXiv:1005.2378 [hep-ph].

[66] E. Braidot, arXiv:1102.0931 [nucl-ex].

[67] A. Stasto, B. W. Xiao and D. Zaslavsky, arXiv:1204.4861 [hep-ph].

[68] F. Dominguez, B. -W. Xiao and F. Yuan, Phys. Rev. Lett. **106** (2011) 022301 [arXiv:1009.2141 [hep-ph]].

[69] F. Dominguez, C. Marquet, B. -W. Xiao and F. Yuan, Phys. Rev. D **83** (2011) 105005 [arXiv:1101.0715 [hep-ph]].

[70] E. Avsar, arXiv:1203.1916 [hep-ph].

[71] K. Kutak, K. Golec-Biernat, S. Jadach and M. Skrzypek, JHEP **1202** (2012) 117